

Investigation of the Viscosity and Structural Properties of CaO-SiO₂-TiO₂ Slags

KAI ZHENG, ZUOTAI ZHANG, LILI LIU, and XIDONG WANG

The viscosity of CaO-SiO₂-TiO₂ slags was measured *via* the rotating cylinder method to reveal the effect of TiO₂ on viscous flow of the slags. Furthermore, the structure of the ternary slags and the role of Ti⁴⁺ were investigated by Fourier transform infrared and Raman spectroscopy techniques. The results are beneficial for a better understanding of the behaviors of Ti-bearing silicate slags. The TiO₂ additions lowered the viscosity and apparent activation energy of the slags. However, the degree of polymerization (DOP) of silicate network was found to be enhanced with increasing the TiO₂ content, which is suggested by the increase in mole fraction of Q^3 ([SiO₄]-tetrahedra with three bridging oxygens) and the decrease in Q^0 . The Eq. [2] $Q^2 \leftrightarrow Q^1 + Q^3$ was appropriate to express the relationship of different Q^n species. The introduction of Ti⁴⁺ into the silicate network as network formers increased the DOP but weakened the strength of slag structure at the same time. Besides, a large proportion of Ti⁴⁺ exists in the slag in the form of TiO_4^{4-} monomers, resulting in a decrease of viscosity with increasing TiO₂ content.

DOI: 10.1007/s11663-014-0053-8

© The Minerals, Metals & Materials Society and ASM International 2014

I. INTRODUCTION

TiO₂-containing slags are significant in the processes of ironmaking, steelmaking, and Ti-recycling industries. In the continuous casting of steel, TiO₂ is widely used as one of the most important component to replace CaF₂ in mold fluxes, since fluorides will cause severe damage to equipment and pollute the environment.^[1] Analogous to the role of CaF₂, the addition of TiO₂ exerts a deep influence on the viscosity of fluoride-free mold fluxes to provide lubrication between the steel and the mold.^[2,3] Moreover, slags containing the CaO-SiO₂-TiO₂ (CST) system are considered to have the heat-transfer function because the crystallization ability of crystals such as CaO·SiO₂·TiO₂ or CaTiO₃ is comparable to cuspidine (3CaO·2SiO₂·CaF₂) in commercial mold fluxes.^[2,4,5] Therefore, slags containing the CST system are proposed as the most promising candidate for fluoride-free mold flux.

Titanium resources are comparatively abundant in China, and most of them exist in the form of vanadium-titanium magnetite (VTM) ore. A complete set of blast furnace processes is adopted to extract metal from the VTM ore. In this process, most of iron and part of vanadium are reduced into the hot metal, while nearly

all Ti components are left in the blast furnace slag. During the Ti recycling process, it is necessary to concentrate the entire Ti element in the slag into a certain Ti-containing phase such as anosovite and perovskite under chosen conditions.^[6-8] As one of the most important physical properties of slag, the viscosity is closely related to the crystallization behavior of molten slag. Understanding the viscosity behaviors of slags with different contents of TiO₂ is also essential in optimizing the operations for continuous-casting and blast-furnace processes.^[9,10] It is well known that the macroscopic physical and chemical properties of slags are primarily determined by the microscopic structures. Consequently, to discover the mechanism of the influence of TiO₂ addition on the viscosity of silicate slags, it is of crucial importance to analyze the structure of TiO₂-bearing slags in detail, especially the role and coordination condition of Ti⁴⁺.

Previous studies mainly concentrated on the slags with complex compositions and relatively small ranges of TiO₂ content,^[3,11-13] and the existence of some extra oxides such as Al₂O₃, B₂O₃, and MgO makes it difficult to execute a penetrating analysis into the structural role of Ti in slags. However, the research work on the property and structure of the ternary CST system is very limited. In this article, we focused attention on seven CST slag samples with a fixed basicity ($R = w(\text{CaO})/w(\text{SiO}_2)$) equal to 1.2 and a broad range of TiO₂ content from 0 to 30 wt pct, and the compositions were simplified from typical industrial Ti-bearing blast-furnace slags in China.^[10] The slag viscosities were measured by rotating cylinder method and the structure information of quenched slags was acquired by Fourier transform infrared (FTIR) and Raman spectroscopy. The study of these CST samples will surely provide us some new insights into the role of TiO₂ in slags and will

KAI ZHENG, Master Degree Candidate, is with the Department of Energy and Resource Engineering, College of Engineering, Peking University, Beijing 100871, P.R. China. ZUOTAI ZHANG and XIDONG WANG, Professors, and LILI LIU, Doctor, are with the Department of Energy and Resource Engineering, College of Engineering, Peking University, and also with the Beijing Key Laboratory for Solid Waste Utilization and Management, Peking University. Contact e-mail: zuotaizhang@pku.edu.cn

Manuscript submitted October 28, 2013.

Article published online March 22, 2014.

facilitate the application of Ti-bearing slags in the related industrial processes.

II. EXPERIMENTAL METHOD

The target compositions of the seven slag samples are listed in Table I. Analytical-grade CaO, SiO₂, and TiO₂ were taken as raw materials, which were thoroughly mixed in an agate mortar before melting. Then, about 180 g mixtures with different compositions were placed into a molybdenum crucible and premelted in a vertical tubular furnace. The samples were preserved at 1823 K (1550 °C) under purified Ar atmosphere for 2 hours to ensure completely molten and homogenized slags. The liquid slags were subsequently quenched and crushed for viscosity measurement. The compositions of quenched slags were confirmed by X-ray fluorescence analysis, as shown in Table I.

The viscosity measurements were carried out by the rotating cylinder method using a Brookfield digital viscometer and the schematic experimental apparatus is shown in Figure 1. The working spindle and crucible were made of molybdenum and connected to the viscometer by an alumina shaft. An electric resistance furnace with six U-shape MoSi₂ heating elements was employed. A Pt-10 pct Rh/Pt thermocouple protected by an alumina tube was placed beneath the bottom of the crucible to monitor the experimental temperature. The viscometer was calibrated using different silicone oil standards with known viscosities at 298 K (25 °C).

The Mo crucible filled with 140 g premelted slag was put at the constant temperature zone of the furnace. Ar gas was inlet into the reaction chamber at a flow rate of 0.3 NL/min throughout the experimental process to prevent the oxidation of the spindle and crucible. The furnace was heated up to 1823 K (1550 °C) at a heating rate of 5 K/min and held for 1 hour to guarantee slag homogenization and temperature stabilization. Then, the spindle was carefully immersed into the molten slag and maintained at 10 mm above the crucible base. The spindle and crucible were aligned along the axis of the viscometer. All viscosity measurements were performed during the cooling cycles. Before each measurement, the liquid slag was preserved at the corresponding temperature for 30 minutes to ensure thermal equilibrium. Three different rotating speeds were used for each

measurement and the equilibrium time at each rotating speed was about 2 minutes. The variation of viscosity values at relatively high temperatures due to speed changes was less than 3 pct, indicating that the molten slag was Newtonian-type fluid. When the temperature dropped to a certain degree, this variation was sometimes larger than 3 pct, indicating that the slag was no longer Newtonian type. Thus, the average values of the results at three rotating speeds were adopted as the final viscosity data. Replicate experiments were conducted on CST2 and CST4 to verify reproductivity of the results.

After finishing the viscosity measurements, the slags were reheated to 1823 K (1550 °C) and held for 1 hour, and then they were quenched by water to obtain the glass phase of slag samples. The X-ray diffraction (XRD) curves shown in Figure 2 indicate the glass

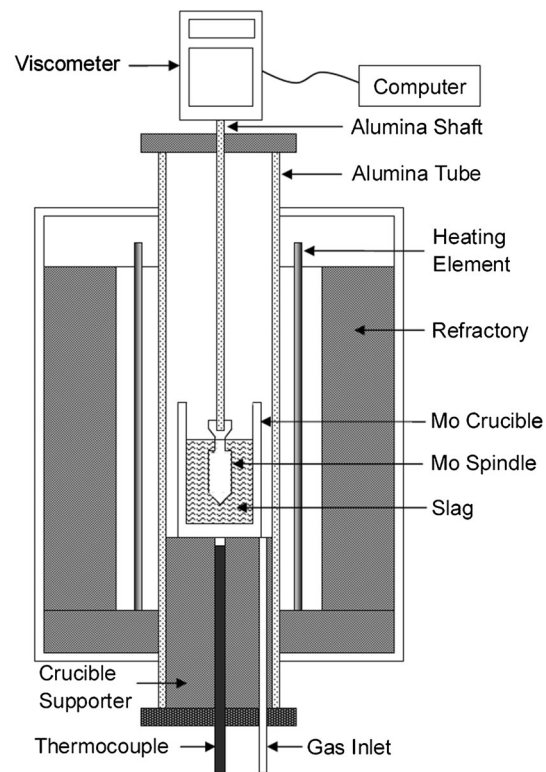


Fig. 1—Experimental apparatus for the measurement of slag viscosity.

Table I. Oxide Compositions of Experimental Slag Samples

Slag	Initial Composition (Wt Pct)				Final Composition by XRF (Wt Pct)				
	CaO	SiO ₂	TiO ₂	R	CaO	SiO ₂	TiO ₂	Others*	R
CST1	54.55	45.45	0	1.2	53.43	46.27	0	0.30	1.15
CST2	51.82	43.18	5	1.2	51.39	43.46	4.74	0.41	1.18
CST3	49.09	40.91	10	1.2	48.47	41.65	9.45	0.43	1.16
CST4	46.36	38.64	15	1.2	46.00	39.21	14.37	0.42	1.17
CST5	43.64	36.36	20	1.2	42.57	36.42	20.62	0.39	1.17
CST6	40.91	34.09	25	1.2	40.32	34.42	24.88	0.38	1.17
CST7	38.18	31.82	30	1.2	37.69	31.22	30.75	0.34	1.21

*The category "others" included Al₂O₃, MgO, etc., which were introduced into the slag from raw materials. XRF = X-ray fluorescence.

samples to be totally amorphous and representative of the structure of molten slags. FTIR spectroscopy (VECTOR 22, Bruker Corporation, Germany) was employed to analyze the glass structures with a resolution of 1 cm^{-1} over the spectral range of 4000 to 400 cm^{-1} . Twenty-four scans were collected for each sample. The glass samples were finally tested by a laser confocal Raman spectrometer (JY-HR80, Jobin Yvon, France) at room temperature with excitation wavelength of 532 nm and a 1-mW semiconductor laser as the light source. The Raman spectra were recorded in the range of 100 to 2000 cm^{-1} and the precision of wave number is 1 cm^{-1} .

III. RESULTS AND DISCUSSION

A. Effect of Temperature and TiO_2 Content on the Slag Viscosity

The measured viscosity data of CST slags at various temperatures are displayed in Table II. The viscosity data of each sample were recorded during the cooling cycle until a sudden increase emerges in the viscosity values. According to Sridhar *et al.*,^[14] the appearance of this inflection point in viscosity could be attributed to the initial precipitation of crystal phases in the melt, and the corresponding temperature point is referred to as the break temperature, below which the slag becomes

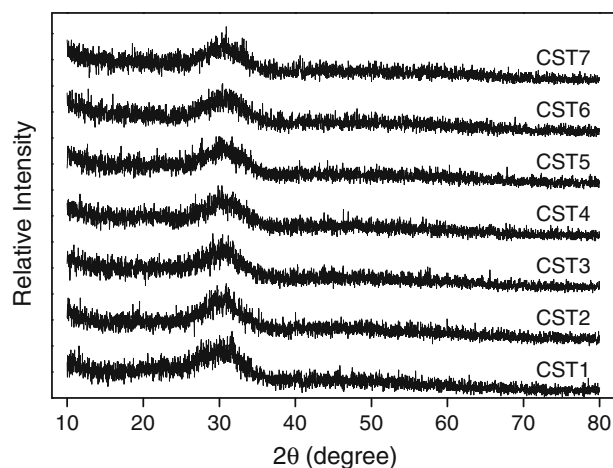


Fig. 2—XRD curves of the quenched samples.

non-Newtonian in behavior. Figure 3 illustrates the viscosity for several samples as a function of temperature, and the inflection point of viscosity data can be easily identified for each sample. Thus, the variation of break temperature with TiO_2 content is deduced from the positions of inflection points, which are also marked in Table II. The break temperature of CST slags decreases from $\sim 1763 \text{ K}$ to $\sim 1713 \text{ K}$ ($1490 \text{ }^\circ\text{C}$ to $1440 \text{ }^\circ\text{C}$) with the TiO_2 content increasing from 0 to 20 wt pct, whereas increases to $\sim 1738 \text{ K}$ ($1465 \text{ }^\circ\text{C}$) with further increase of TiO_2 content to 30 wt pct. In fact, the current slag samples with designed compositions are located in different regions of the equilibrium phase diagram of $\text{CaO-SiO}_2\text{-TiO}_2$ system, and the primary crystalline regions change from $\alpha\text{-CaSiO}_3$ to CaTiO_3 with increasing TiO_2 content.^[15] Therefore, the nonmonotonous changing of break temperature with TiO_2 addition is mainly due to the distinctions in crystallization behavior for slags with different compositions.

The viscosity of CST system has been reported by a number of previous works.^[16–19] Among those studies, the results by Dingwell^[16] were obtained under well-controlled conditions and demonstrated to be most accurate and credible.^[20] Dingwell investigated the viscosity of $\text{CaSiO}_3\text{-TiO}_2$ slags with TiO_2 content ranging from 10 to 80 mol pct, and the vast majority of viscosity data are comparable with the current results

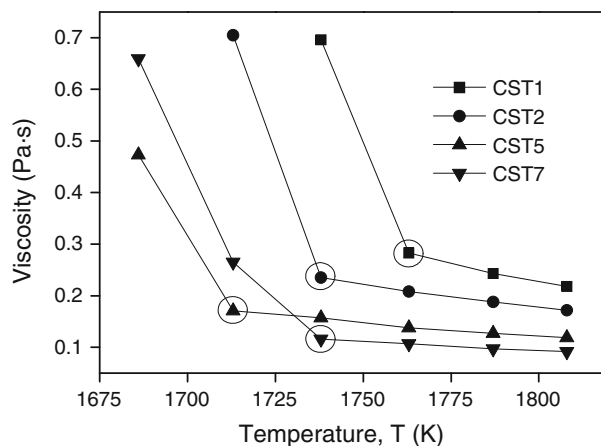


Fig. 3—Viscosities of CST1, CST2, CST5, and CST7 vs temperature. The data of CST3, CST4, and CST6 are not shown in the figure to guarantee clarity. Circles mark the inflection points and lines are guides to the eyes.

Table II. Measured Viscosities (Pa s) of CST Slags in Various Temperatures

Slag	1808 K (1535 °C)	1787 K (1514 °C)	1763 K (1490 °C)	1738 K (1465 °C)	1713 K (1440 °C)	1686 K (1413 °C)
CST1	0.218	0.243	0.283*	0.696	—	—
CST2	0.172	0.188	0.208	0.235*	0.705	—
CST3	0.147	0.156	0.172	0.193*	0.355	—
CST4	0.131	0.137	0.148	0.171	0.189*	0.342
CST5	0.119	0.127	0.138	0.157	0.171*	0.473
CST6	0.099	0.106	0.116	0.128*	0.296	0.725
CST7	0.092	0.097	0.107	0.116*	0.265	0.659

Note: The asterisks (*) in the table mark the positions of inflection points.

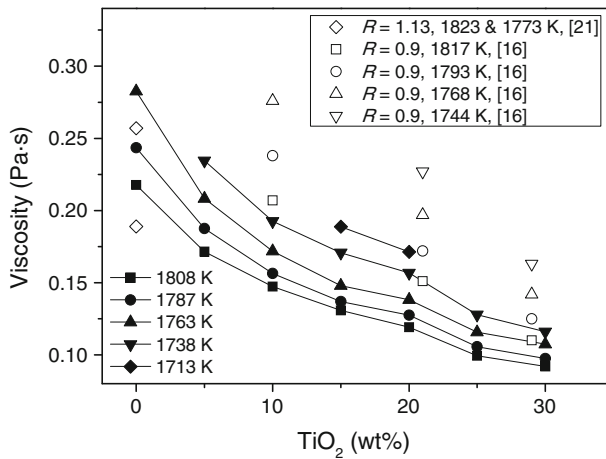


Fig. 4—Viscosity in the fully liquid region varying with TiO_2 content at different temperatures. Comparable data from works of other researchers are included. Lines are guides to the eyes.

considering that the basicity of our samples ($R = 1.2$) is relatively larger (Figure 4). It should be mentioned that the viscosity of CST1 also agrees well with other published data on the CaO-SiO_2 binary melts.^[21,22] The viscosity of CST1 (binary slag with basicity equal to 1.15 by XRF) equals 0.218, 0.243, and 0.283 Pa s at 1808 K, 1787 K, and 1763 K (1535 °C, 1514 °C, and 1490 °C), respectively, and the value for binary melt with similar basicity ($R = 1.13$) reported by Bockris and Lowe^[21] was 0.189 and 0.257 Pa s at 1823 K and 1773 K (1550 °C and 1500 °C), respectively.

The effect of TiO_2 on the viscous behavior of CST slags at different temperatures is plotted in Figure 4, where only the viscosity data in fully liquid region of slag system and some comparable data by other researchers are included. In this figure, the slag viscosity decreases with the increase of TiO_2 content at studied temperature range, which is consistent with most of the previous works. Shankar *et al.*^[11] investigated the viscosities of $\text{CaO-SiO}_2\text{-MgO-Al}_2\text{O}_3$ and $\text{CaO-SiO}_2\text{-MgO-Al}_2\text{O}_3\text{-TiO}_2$ slags and observed that the viscosity for slags with different basicities (0.8 and 0.5) decreased with a small addition of ~ 2 wt pct TiO_2 . Saito *et al.*^[23] found that the viscosity of $\text{CaO-SiO}_2\text{-Al}_2\text{O}_3\text{-TiO}_2$ slag decreased significantly with the TiO_2 concentration increasing from 10 wt pct to 20 wt pct. Dingwell^[16] stated that the logarithm of the viscosity value of $\text{CaSiO}_3\text{-TiO}_2$ slag melt decreased linearly with the addition of TiO_2 . Some explanations are given below whose validity in our samples was not confirmed. As many researchers have pointed out,^[3,10,24] the decrease of viscosity with TiO_2 addition may suggest that some Ti^{4+} play the role of network modifier in silicate slags to break the silicate network. However, the structural role of Ti^{4+} in silicate slag and glass is still on debate,^[25-27] and the slag structure could be loosened by the formation of Ti-O-Ti linkages along with TiO_4^{4-} monomers.^[3,28] Therefore, it cannot be decided whether the conclusions of previous works are applicable to our slag system before structure analysis, and the discussions on the links of viscosity and slag structure are given after

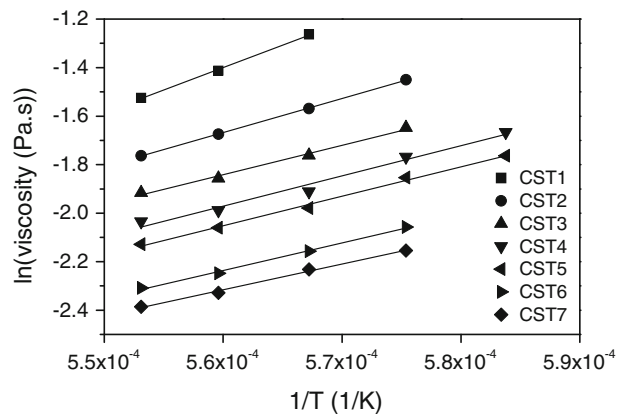


Fig. 5—Natural logarithm of the viscosity in fully liquid region for CST slags vs reciprocal temperature. Lines are linear fitting results of the data.

Raman spectral analysis. It is noteworthy in Figure 4 that the effect of TiO_2 on viscosity is most pronounced for the first addition of 5 wt pct TiO_2 indicated by the slope of the curves. Similar results were obtained by Sohn *et al.*^[24] and Park *et al.*^[12] Because the first TiO_2 addition has already loosened the slag structure to some extent, the subsequent increase of TiO_2 has comparatively less effect on decreasing the viscosity.^[24]

The relationship between the slag viscosity and temperature can be described by the Arrhenius-type equation:

$$\eta = A \exp(E_\eta/RT), \quad [1]$$

where A , E_η , R , and T denote the pre-exponential factor, apparent activation energy for viscous flow, universal gas constant, and absolute temperature, respectively. E_η represents the energy barrier that the cohesive flow units in slags have to overcome when the units move between different equilibrium states.^[22] The variation of E_η suggests structure changes in slags, and its value is expected to be constant for a certain slag melt system before precipitation happens. Figure 5 exhibits natural logarithm of the viscosity in fully liquid region for all 7 CST slags vs reciprocal temperature, including the linear fitting results of the data. The E_η values are therefore evaluated from slope of the lines according to the Arrhenius relationship and displayed in Table III. It is shown that E_η decreases with increasing TiO_2 content, indicating the reduction of energy barrier for viscous flow and the formation of some simpler structural units in slags.^[3] Besides, the decline in E_η value is also most prominent when TiO_2 concentration increases from 0 to 5 wt pct, resembling the variation tendency of viscosity vs TiO_2 content shown in Figure 4.

From the above results, it can be summarized that the slag structure is simplified due to the increase of TiO_2 concentration, although the details are still uncertain. On the other hand, because Ti^{4+} cation is larger in size and smaller in electronegativity comparing with Si^{4+} cation, the Ti-O bonds are expected to be weaker than Si-O bonds. So the strength of structural network will decline if Ti^{4+} cations are incorporated into silicate network, playing the role of decreasing viscosity.^[20]

Therefore, to reveal the detailed mechanism of viscosity change with TiO_2 and the existence form of Ti^{4+} in slag, it is required for a deep insight into the microscopic structure of CST slags.

B. FTIR Spectra of CST Slags

Before studying structural details, it is necessary to clarify that the slag structure is not significantly affected by quenching process, which is confirmed by Seifert *et al.*^[29] The FTIR spectral curves are plotted in Figure 6, where three regions are partitioned from ~ 420 to $\sim 1250 \text{ cm}^{-1}$, including a strong broad band in the high-wavenumber region from ~ 770 to $\sim 1250 \text{ cm}^{-1}$, a weak shoulder from ~ 610 to $\sim 770 \text{ cm}^{-1}$ in close vicinity of the broad band, and a relatively intense band in the low-wavenumber region from ~ 420 to $\sim 610 \text{ cm}^{-1}$. The broad band between ~ 770 to $\sim 1250 \text{ cm}^{-1}$ has been generally assigned to the symmetric stretching vibrations of $[\text{SiO}_4]$ -tetrahedra in the three-dimensional silicate network.^[30,31] The individual bands reflecting different types of Q^n species (n equals to the number of bridging oxygens (BOs) in one $[\text{SiO}_4]$ -tetrahedron, ranging from 0 to 4) are located at the positions of ~ 850 , ~ 900 , 950 – 1000 , ~ 1050 , and $\sim 1200 \text{ cm}^{-1}$, respectively.^[32] The band for fully polymerized $[\text{SiO}_4]$ (Q^4) is not detected in FTIR spectra, and the positions of Q^0 , Q^1 , Q^2 , and Q^3 are labeled in Figure 6. No obvious changes with TiO_2 addition are observed in the width and depth of this broad band, yet its center shifts to higher wavenumber region and the peak position rises from 989 to 1003 cm^{-1} , indicating that the concentration of Q^3 units in silicate network is raised by TiO_2 addition comparing with the concentration of less polymerized units. Moreover, there is a small shoulder at $\sim 850 \text{ cm}^{-1}$ in the curves of first few

Table III. Calculated Apparent Activation Energy (E_a , kJ/mol) for Slag Samples

CST1	CST2	CST3	CST4	CST5	CST6	CST7
154	117	101	104	101	95	88

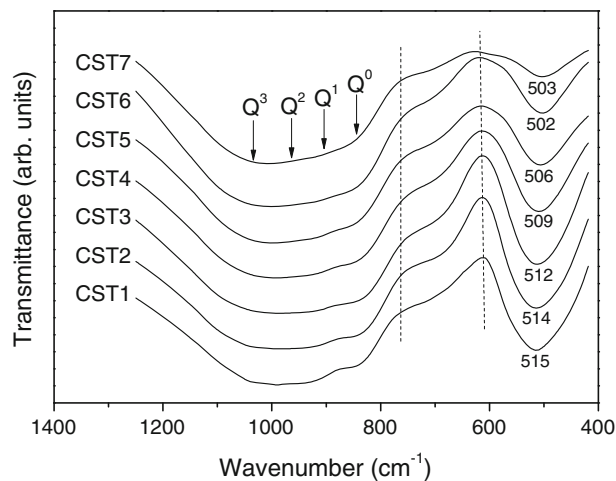


Fig. 6—FTIR transmittance of quenched CST samples as a function of wavenumber.

samples. The shoulder gradually becomes shallower and finally vanishes in the last three slag samples. Because this shoulder represents the band of Q^0 species, it can be concluded that the concentration of Q^0 (SiO_4^{4-} -monomers) diminishes and the silicate network becomes more polymerized with increasing TiO_2 content.

According to McMillan^[32] and Virgo *et al.*,^[33] the shoulder beside the broad band centered at $\sim 700 \text{ cm}^{-1}$ is due to the symmetric stretching motion of the bridging oxygen in dimer units ($\text{Si}_2\text{O}_7^{6-}$) within the slag structure. It seems that there are no noticeable changes in the position and intensity of this shoulder. McMillan^[34] stated that the bands between 400 and 650 cm^{-1} were associated with the presence of BOs, which acted as corners shared by adjacent $[\text{SiO}_4]$ -tetrahedra, and the wavenumbers of these bands were sensitive to the Si-O-Si bond angle. In our samples shown in Figure 6, the peak value in this region reduces gradually from 515 to 503 cm^{-1} , suggesting a more polymerized silicate network with TiO_2 increasing proposed by McMillan.^[34] The decrease in the intensity of the bands from CST1 to CST7 is simply attributed to the decrease of silicate weight fraction in the slag samples. The slag viscosity decreases with increasing TiO_2 content despite an increase in the degree of polymerization (DOP) of the silicate network. So, some other factors must have significant influences on the slag viscosity, which will be given in the subsequent discussions.

C. Raman Spectra of CST Slags

Figure 7 exhibits the Raman curves of the seven CST samples. The spectral curve of CST1 without TiO_2 is divided into two regions, *i.e.*, the higher frequency region between 800 and 1200 cm^{-1} and lower frequency region between 600 and 800 cm^{-1} . A band centered at $\sim 660 \text{ cm}^{-1}$ appears in the low-frequency region. In the high-frequency region, the two peaks are located at 963 and 860 cm^{-1} , respectively, and a shoulder at $\sim 920 \text{ cm}^{-1}$ exists between those two peaks. In the CaO-SiO₂ binary melt with analogous composition (mole ratio of CaO to SiO₂ is 1.18) studied by Mysen *et al.*,^[35] two peaks were also observed at nearly 950 and 850 cm^{-1} , although the intensity of the peak at 950 cm^{-1} was relatively stronger than the peak at 963 cm^{-1} in CST1. This high-frequency region appeared in many previous works focusing on silicate slags and glasses with different components and compositions.^[10,12,32] However, the addition of only 5 wt pct TiO_2 to the binary silicate slag causes significant changes to the spectral curve. First, only the peak around 850 cm^{-1} remains in CST2 with higher intensity and greater width, while the peak at $\sim 960 \text{ cm}^{-1}$ becomes lower than the shoulder at $\sim 920 \text{ cm}^{-1}$. Second, some new bands between ~ 700 and $\sim 800 \text{ cm}^{-1}$ are introduced to the Raman curve of CST2, for the reason that the gap at about 800 cm^{-1} in CST1 disappears and the envelope between 600 and 800 cm^{-1} turns into a shoulder beside the peak. With the continuous increase of TiO_2 content, the shoulder at $\sim 700 \text{ cm}^{-1}$ disappears and the peak position shifts from $\sim 845 \text{ cm}^{-1}$ in CST3 to $\sim 820 \text{ cm}^{-1}$ in CST7. The shoulder in the range of 900 to 980 cm^{-1} becomes less pronounced with the addition of TiO_2 ,

which is reasonable taking into account that this frequency region is related to silicate network and the concentration of SiO_2 becomes smaller.

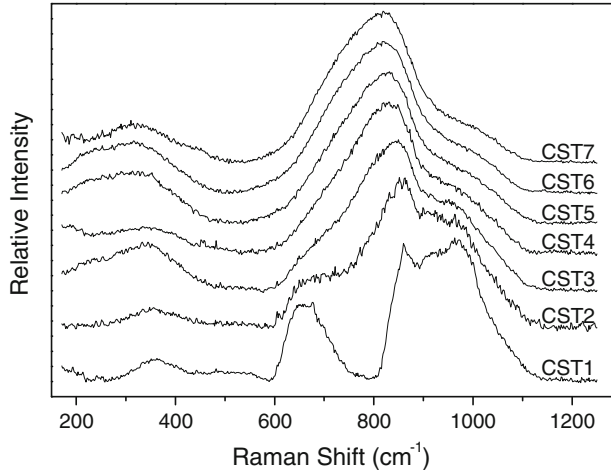


Fig. 7—Raman spectral curves of quenched CST samples.

Deconvolution of the Raman curves is essential to carry out detailed investigation into the slag structure. The fitting process was conducted under the guidance of the work performed by Mysen *et al.*^[35] First, all bands comprising the Raman envelope were assumed to be symmetric and to obey Gaussian distribution. Second, the bands were fitted to the envelope only when their existence was indicated by distinguishable peaks or shoulders, or by abrupt deviations between the sum of prefitting bands and the original curve. The envelope between 600 and 800 cm^{-1} in CST1 is derived from the presence of Si-O-Si linkages, while the Raman signal between 800 and 1150 cm^{-1} represents the symmetric stretching vibration of $[\text{SiO}_4]$ -tetrahedra in silicate network. Mysen *et al.*^[35] assigned the bands at the region of 840 to 860, 900 to 920, 960 to 980, and $\sim 1050 \text{ cm}^{-1}$ to the presence of Q^0 , Q^1 , Q^2 , and Q^3 species, respectively. Therefore, considering the features of the Raman curve as well as some previous works, the high-frequency region in CST1 is deconvoluted into four symmetric bands at ~ 850 , ~ 905 , ~ 975 , and $\sim 1050 \text{ cm}^{-1}$, representing Q^0 , Q^1 , Q^2 , and Q^3 structural units, as

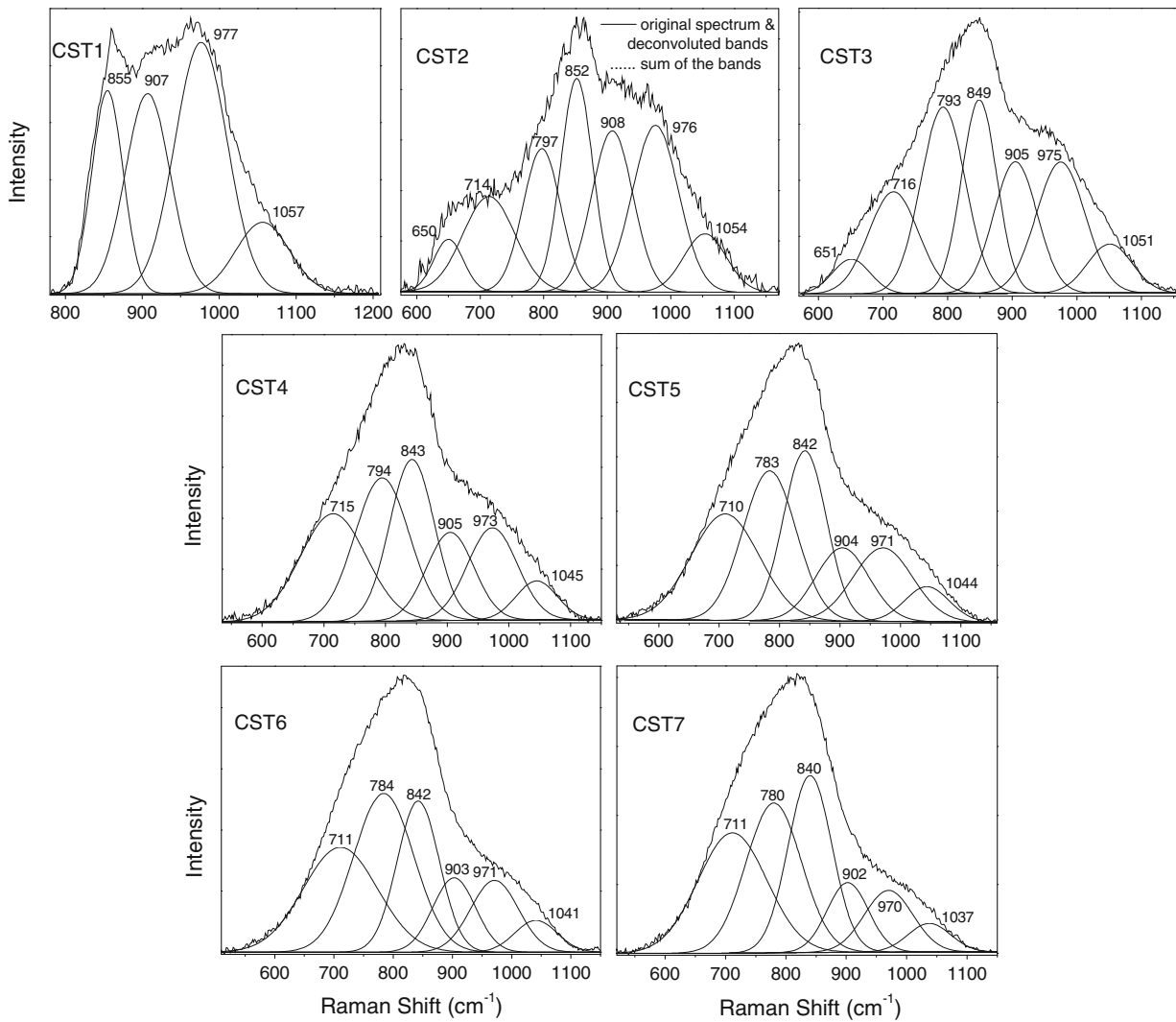


Fig. 8—Deconvoluted results of the Raman spectral curves for CST samples.

illustrated in Figure 8. These four bands are preserved in the rest of the samples but with different frequencies and intensities, and Q^4 is not observed in any of our samples because the signal between 1150 and 1200 cm^{-1} was barely detected. In CST2, a new band related to Ti arises near 800 cm^{-1} to fill up the gap in curve of CST1, and the shoulder in the low-frequency region are formed by two bands at ~ 650 and ~ 710 cm^{-1} . As shown in Figure 8, the bands at ~ 710 and ~ 800 cm^{-1} are inherited in the rest five samples with the band at ~ 650 cm^{-1} remaining only in CST3. The reflection of 650 cm^{-1} band in CST2 and CST3 is same as the band between 600 and 800 cm^{-1} in CST1. The assignments of the rest bands will be discussed below.

D. Interpretation of Slag Structure

The abundance of the coexisting structural units can be deduced from the areas of corresponding Raman bands. But it is incorrect to calculate the fraction of Q^n species by directly comparing the band areas because different Q^n species have different polarizabilities, and the mole fraction of Q^n species can only be worked out by calibrating the band area using Raman scattering coefficient, which is independent of temperature and only decided by the Q^n species themselves.^[36] The mole fractions are related to the band areas according to the equation: $X_i = \theta_i A_i$ ($i = 0$ to 3), where X_i , θ_i , and A_i denote the mole fraction of Q^i , Raman scattering coefficient, and band area of Q^i , respectively.

The band at ~ 850 cm^{-1} is assigned to Q^0 in CST1. However, the intensity of this band seems to continuously increase with increasing TiO_2 content. To verify this point of view, we compare the area of the ~ 850 cm^{-1} band with the other three bands and find that with TiO_2 addition from 0 to 30 wt pct, A_0/A_3 increases from 1.66 to 6.12, A_0/A_2 increases from 0.48 to 2.49, A_0/A_1 increases from 0.71 to 2.59, respectively. Thus, if this band in seven samples is always assigned to Q^0 species, the mole fraction of Q^0 (X_0) is believed to increase continuously because θ_0 , θ_1 , θ_2 , and θ_3 are constants, which is inconsistent with FTIR results that the concentration of Q^0 diminishes. Therefore, some other structural units must also contribute to the Raman

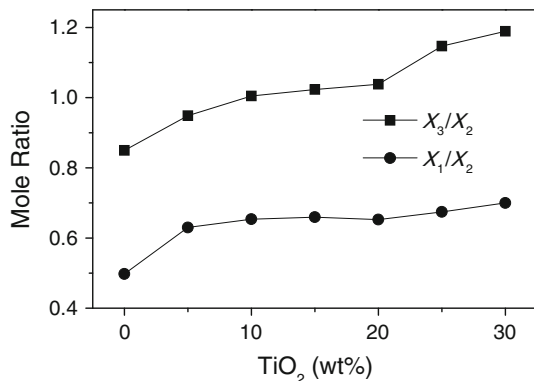


Fig. 9—Mole ratio of Q^3 to Q^2 and Q^1 to Q^2 as the function of TiO_2 content.

signal at ~ 850 cm^{-1} . By reviewing previous literature,^[12,37] we deem that the band at ~ 850 cm^{-1} also reflects the stretching vibration of Ti-O bond in $\text{Ti}_2\text{O}_6^{4-}$ chain units, which compete with silicate to coordinate Ca^{2+} so as to maintain local charge balance. Consequently, a few NBOs linked to Si^{4+} turn into BOs, increasing the DOP of silicate network.

The bands at ~ 905 , ~ 975 , and ~ 1050 cm^{-1} are assigned to Q^1 , Q^2 , and Q^3 units, respectively. Although the accurate values for θ_i still remain unknown, the ratios of Raman scattering coefficients θ_3/θ_2 and θ_1/θ_2 were computed by Mysen *et al.*^[38] and Frantz *et al.*^[36] via comparing the nuclear magnetic resonance data with Raman data of silicate systems. The mole ratios of Q^n species are given by the following equations:

$$X_3/X_2 = (\theta_3/\theta_2) (A_3/A_2) = 2.92 (A_3/A_2), \quad [2]$$

$$X_1/X_2 = (\theta_1/\theta_2) (A_1/A_2) = 0.73 (A_1/A_2). \quad [3]$$

The variations of X_3/X_2 and X_1/X_2 with TiO_2 concentration are plotted in Figure 9, where X_3/X_2 increases monotonically as already indicated by the FTIR curves, and X_1/X_2 also increases but to a smaller extent. Therefore, the expression [2] $Q^2 \leftrightarrow Q^1 + Q^3$ is suitable to describe the relationship among Q^n species, and the gross polymerization of silicate network is enhanced by the increase of TiO_2 . It is worth noting that the increase of X_1/X_2 is most pronounced between CST1 and CST2 just as the variation tendency of viscosity.

Table IV displays the frequencies of the Q^1 , Q^2 , and Q^3 bands varying with TiO_2 content, and the decreases of frequencies are found in all three bands. Analogous trends were observed in the Raman spectra of Ti-bearing sodium silicate melts.^[25] Neuville *et al.*^[39] found the decreasing frequencies of Q^n bands with increasing Al/Si ratio in aluminosilicate glass and contributed this trend to the substitution of Al^{3+} for Si^{4+} in tetrahedral coordination due to the weaker strength of the Al-O bond. Because the bond strength of Ti-O is also weaker than Si-O, the decrease in frequencies indicates that a considerable proportion of Ti^{4+} is introduced into the silicate network as the network formers, giving rise to a higher DOP but a weaker strength of polymerization. Additionally, the O-Ti-O linkages will be brought into the slag structure by the introduction of Ti^{4+} into silicate network. Mysen *et al.*^[40] and Wang *et al.*^[37] proposed that the bands at ~ 710 cm^{-1} in the spectra of Ti-bearing CaSiO_3 melt reflected the O-Ti-O deformation. So we

Table IV. Frequencies (cm^{-1}) of Q^1 , Q^2 , and Q^3 Bands in the Raman Spectra of CST Slags

Slag	Q^3	Q^2	Q^1
CST1	1057	977	907
CST2	1054	976	908
CST3	1051	975	905
CST4	1045	973	905
CST5	1044	971	904
CST6	1041	971	903
CST7	1037	970	902

Table V. The Recommended Assignments of Ti-Related Raman Bands

Frequencies (cm ⁻¹)	Recommended Assignments
~850	stretching vibrations of Ti-O bonds in $Ti_2O_6^{4-}$ chain units, and Q^0 species in silicate network
~790	Ti-O stretching vibrations in TiO_4^{4-} monomers
~710	deformation of O-Ti-O or O-(Si,Ti)-O in chain or sheet units or both

assign the ~710 cm⁻¹ band to deformation of O-Ti-O or O-(Si,Ti)-O in chain or sheet units or both. This band is quite broad in the last four Raman curves shown in Figure 8, suggesting that O-Ti-O linkages have been formed in different structural units.

The decrease of apparent activation energy for viscous flow (E_η) confirms the formation of some simpler structural units in slags, while DOP increases and the fraction of SiO_4^{4-} monomer decreases with the TiO_2 content. To solve this contradiction, we assign the intense bands between 780 and 800 cm⁻¹ to the stretching vibration of Ti-O in TiO_4^{4-} monomers with support from the works done by Mysen *et al.*^[40] and Sakka *et al.*^[28] The great intensity of this band implies that TiO_4^{4-} monomers always make up a large proportion of Ti^{4+} in slags, and they also need charge compensation by Ca^{2+} . The recommended assignments of titanium-associated Raman bands are now gathered in Table V.

A brief summary of the structure of our slag samples is given to explain the reason for the decrease of slag viscosities with increasing TiO_2 content. As shown in the FTIR curves, the shoulder representing the band of Q^0 species becomes shallower and the peak value in low-wavenumber region gradually reduces from 515 to 503 cm⁻¹ with the addition of TiO_2 . The concentration of Q^3 increases compared with other structural units. These three variation trends both indicate that the silicate network becomes more polymerized due to the increase of TiO_2 .^[32,34] From the deconvoluting results of Raman spectra, we observe also that the mole fraction ratio of Q^3 to Q^2 (X_3/X_2) increased monotonically. However, the introduction of Ti^{4+} into the silicate network weakens the strength of polymerization because Ti-O bonds are weaker than Si-O bonds, indicated by the decrease of the frequencies of Q^1 , Q^2 , and Q^3 bands. Moreover, the Raman bands related to Ti manifest that large amounts of simpler and smaller structural units are brought into the slags by TiO_2 addition, such as TiO_4^{4-} monomers and $Ti_2O_6^{4-}$ chains units. Therefore, even though the DOP of slag structure increases, the viscosity of CST slags and apparent activation energy for viscous flow both decrease with TiO_2 addition due to weaker bonds in the network and simpler units in the slags.

IV. CONCLUSIONS

The CaO-SiO₂-TiO₂ slags with a relatively high basicity 1.2 were investigated by measurements of

viscosity combined with FTIR and Raman spectroscopy techniques to clarify the effect of TiO_2 on the viscous flow and structure of silicate slags. The conclusions are as follows:

- (1) The break temperature of slags is decided by their compositions and crystallization behavior. Slag viscosity and apparent activation energy both decrease with increasing TiO_2 content, indicating the formation of some simpler structural units.
- (2) The introduction of Ti^{4+} into silicate network as network formers and the existence of $Ti_2O_6^{4-}$ chain units give rise to a higher DOP for silicate network, demonstrated by the decrease in mole fraction of Q^0 species and the increase in Q^3 species.
- (3) The strength of silicate network is weakened by the introduction of Ti^{4+} , and a large amount of TiO_4^{4-} monomers was proven to exist in the slag structure. The two factors contribute to the decrease of slag viscosity with increasing TiO_2 concentration.

ACKNOWLEDGMENTS

The authors gratefully acknowledge financial support by the National Natural Science Foundation of China (51172003 and 51074009). Support from the National High Technology Research and Development Program of China (863 Program, 2012AA06A114) and the China National Key Technology R&D Program (2011BAB03B02 and 2011BAB02B05) is also acknowledged.

REFERENCES

1. A.I. Zaitsev, A.V. Leites, A.D. Litvina, and B.M. Mogutnov: *Steel Res.*, 1994, vol. 65, pp. 368–74.
2. G. Wen, S. Seetharaman, P. Tang, X. Qi, and Y. Liu: *ISIJ Int.*, 2007, vol. 47, pp. 1117–25.
3. Z. Wang, Q. Shu, and K. Chou: *Steel Res. Int.*, 2013, vol. 84, pp. 766–76.
4. X. Qi, G. Wen, and P. Tang: *J. Non-Cryst. Solids*, 2008, vol. 354, pp. 5444–52.
5. H. Nakada and K. Nagata: *ISIJ Int.*, 2006, vol. 46, pp. 441–49.
6. J. Li, Z.T. Zhang, and X.D. Wang: *Ironmaking Steelmaking*, 2012, vol. 39, pp. 414–18.
7. J. Li, X.D. Wang, and Z.T. Zhang: *ISIJ Int.*, 2011, vol. 51, pp. 1396–402.
8. L. Zhang, M.Y. Wang, and Z.T. Sui: *ISIJ Int.*, 2006, vol. 46, pp. 458–65.
9. Y. Morizane and R.J. Fruehan: *Metall. Mater. Trans. B*, 1999, vol. 30B, pp. 29–43.
10. J.L. Liao, J. Li, X.D. Wang, and Z.T. Zhang: *Ironmaking Steelmaking*, 2012, vol. 39, pp. 133–39.
11. A. Shankar, M. Görnerup, A.K. Lahiri, and S. Seetharaman: *Metall. Mater. Trans. B*, 2007, vol. 38B, pp. 911–15.
12. H. Park, J.-Y. Park, G.H. Kim, and I. Sohn: *Steel Res. Int.*, 2012, vol. 83, pp. 150–56.
13. S. Ren, J. Zhang, L. Wu, W. Liu, Y. Bai, X. Xing, B. Su, and D. Kong: *ISIJ Int.*, 2012, vol. 52, pp. 984–91.
14. S. Sridhar, K.C. Mills, O.D.C. Afrange, H.P. Lörz, and R. Carli: *Ironmaking Steelmaking*, 2000, vol. 27, pp. 238–42.
15. R.C. DeVries, R. Roy, and E.F. Osborn: *J. Am. Ceram. Soc.*, 1955, vol. 38, pp. 158–71.
16. D.B. Dingwell: *Am. Mineral.*, 1992, vol. 77, pp. 270–74.

17. A. Ohno and H.U. Ross: *Can. Metall. Q.*, 1963, vol. 2, pp. 327–33.
18. M.G. Froberg and R. Weber: *Arch. Eisenhüttenwes*, 1965, vol. 36, pp. 477–80.
19. H. Schenck and M.G. Froberg: *Arch. Eisenhüttenwes*, 1962, vol. 33, pp. 421–25.
20. L. Zhang and S. Jahanshahi: *The Seventh International Conference on Molten Slags, Fluxes and Salts*, 2004, pp. 51–6.
21. J.O'M. Bockris and D.C. Lowe: *Proc. Roy. Soc.*, 1954, vol. 226, pp. 423–35.
22. G. Urbain, Y. Bottinga, and P. Richet: *Geochim. Cosmochim. Acta*, 1982, vol. 46, pp. 1061–72.
23. N. Saito, N. Hori, K. Nakashima, and K. Mori: *Metall. Mater. Trans. B*, 2003, vol. 34B, pp. 509–16.
24. I. Sohn, W. Wang, H. Matsuura, F. Tsukihashi, and D.J. Min: *ISIJ Int.*, 2012, vol. 52, pp. 158–60.
25. B.O. Mysen and D.B. Neuvill: *Geochim. Cosmochim. Acta*, 1995, vol. 59, pp. 325–42.
26. M. Guignard, L. Cormier, V. Montouillout, N. Menguy, D. Massiot, and A.C. Hannon: *J. Phys.*, 2009, vol. 21, p. 375107.
27. M. Roskosz, M.J. Toplis, and P. Richet: *Geochim. Cosmochim. Acta*, 2004, vol. 68, pp. 591–606.
28. S. Sakka, F. Miyaji, and K. Fukumi: *J. Non-Cryst. Solids*, 1989, vol. 112, pp. 64–8.
29. F.A. Seifert, B.O. Mysen, and D. Virgo: *Geochim. Cosmochim. Acta*, 1981, vol. 45, pp. 1879–84.
30. J.H. Park, D.J. Min, and H.S. Song: *Metall. Mater. Trans. B*, 2004, vol. 35B, pp. 269–75.
31. J.H. Park, D.J. Min, and H.S. Song: *ISIJ Int.*, 2002, vol. 42, pp. 344–51.
32. P. McMillan: *Am. Mineral.*, 1984, vol. 69, pp. 645–59.
33. D. Virgo, B.O. Mysen, and I. Kushiro: *Science*, 1980, vol. 208, pp. 1371–73.
34. P. McMillan: *Am. Mineral.*, 1984, vol. 69, pp. 622–44.
35. B.O. Mysen, D. Virgo, and C.M. Scarfe: *Am. Mineral.*, 1980, vol. 65, pp. 690–710.
36. J.D. Frantz and B.O. Mysen: *Chem. Geol.*, 1995, vol. 121, pp. 155–76.
37. Z. Wang, Q. Shu, and K. Chou: *ISIJ Int.*, 2011, vol. 51, pp. 1021–27.
38. B.O. Mysen and J.D. Frantz: *Contrib. Mineral. Petrol.*, 1994, vol. 117, pp. 1–14.
39. D.R. Neuvill, L. Cormier, V. Montouillout, P. Florian, F. Millot, J.-C. Rifflet, and D. Massiot: *Am. Mineral.*, 2008, vol. 93, pp. 1721–31.
40. B.O. Mysen, F.J. Ryerson, and D. Virgo: *Am. Mineral.*, 1980, vol. 65, pp. 1150–65.